Liu *et al. Chem Synth* 2023;3:24
DOI: 10.20517/cs.2023.13

Chemical Synthesis

Research Article

Open Access

Check for updates

Active Pd nanoclusters supported on nitrogen/amino co-functionalized carbon for highly efficient dehydrogenation of formic acid

Dan Liu[1,#], Cheng Zhou[2,#], Ge Wang[2], Yong Li[2], Zhimao Yang[1], Chuncai Kong[1,*], Ben Liu[3,*]

[1]Ministry of Education Key Laboratory for Non-equilibrium Synthesis and Modulation of Condensed Matter, Shaanxi Province Key Laboratory of Advanced Functional Materials and Mesoscopic Physics, School of Physics, Xi'an Jiaotong University, Xi'an 710049, Shaanxi, China.
[2]Beijing Institute of Control Engineering, Beijing 100190, China.
[3]Key Laboratory of Green Chemistry and Technology of Ministry of Education, College of Chemistry, Sichuan University, Chengdu 610064, Sichuan, China.
[#]Authors contributed equally.

***Correspondence to:** Prof. Ben Liu, Key Laboratory of Green Chemistry and Technology of Ministry of Education, College of Chemistry, Sichuan University, Wangjiang Road No. 29, Chengdu 610064, Sichuan, China. E-mail: ben.liu@scu.edu.cn; Prof. Chuncai Kong, Ministry of Education Key Laboratory for Non-equilibrium Synthesis and Modulation of Condensed Matter, Shaanxi Province Key Laboratory of Advanced Functional Materials and Mesoscopic Physics, School of Physics, Xi'an Jiaotong University, Xian Ning West Road No.28, Xi'an 710049, Shaanxi, China. E-mail: kongcc@xjtu.edu.cn

How to cite this article: Liu D, Zhou C, Wang G, Li Y, Yang Z, Kong C, Liu B. Active Pd nanoclusters supported on nitrogen/amino co-functionalized carbon for highly efficient dehydrogenation of formic acid. *Chem Synth* 2023;3:24. https://dx.doi.org/10.20517/cs.2023.13

Received: 1 Mar 2023 **First Decision:** 6 Apr 2023 **Revised:** 19 Apr 2023 **Accepted:** 27 Apr 2023 **Published:** 15 May 2023

Academic Editors: Bao-Lian Su **Copy Editor:** Dong-Li Li **Production Editor:** Dong-Li Li

Abstract

Supported noble metal catalysts have exhibited satisfactory catalytic performance in the dehydrogenation of liquid chemical hydrogen carriers, in which the supports play a paramount role in conditioning the nature of the active center and thus improving the overall reactivity. Herein, the specially designed nitrogen/amino co-functionalized carbon (NH_2-NC) supports are prepared to load active Pd nanoclusters for efficient dehydrogenation of formic acid (FA). The nitrogen/amino co-functionalization of carbon not only facilitates the Pd nanoclusters evenly dispersed with a mean size of 1.4 nm, but also provides a beneficial metal-support interaction to promote FA dehydrogenation. The as-prepared Pd@NH_2-NC discloses a 100% conversion of FA into CO_2 and H_2 with a remarkable initial turnover frequency ($TOF_{initial}$) of 4,892 h^{-1} and a low activation energy (E_a) of 28.5 kJ mol^{-1} without additive at 298 K. The work proposes a co-functionalization strategy to reasonably design supports for heterogeneous catalysts and may be extended to develop other multi-functionalized supports with different compositions and nanostructures.

Keywords: Formic acid, catalysis, hydrogen production, Pd nanocluster, carbon functionalization

INTRODUCTION

Hydrogen storage technologies based on liquid chemical hydrogen carriers have attracted more and more attention due to their safety, convenience, and high efficiency[1-4]. Among them, formic acid (HCOOH, FA) has the advantages of low dehydrogenation reaction enthalpy (30 kJ·mol^{-1}), high hydrogen gravimetric density (4.4 wt %), and volumetric capacity (53.4 g·L^{-1}), a wide range of sources from biomass process and CO_2 reduction, non-toxicity and excellent stability in the liquid state, demonstrating great potential for liquid chemical hydrogen storage[5-8]. The decomposition of FA can take place through two pathways, one is the dehydrogenation process into H_2 and CO_2 and another is the dehydration process into H_2O and CO[9,10]. The CO generated from the dehydration pathway is the undesired product, which will seriously poison noble metal catalysts and lead to a quick deactivation of catalytic performance[11,12]. Furthermore, in order to effectively release H_2, the decomposition of FA requires higher temperature and extra additives (such as HCOONa and $HCOONH_4$), further complicating catalysis[13,14]. Therefore, it is greatly significant to develop desired catalysts with high selectivity and efficiency for FA dehydrogenation under mild conditions.

Pd-based catalysts have displayed remarkable activity toward the dehydrogenation of FA[15-17]. Especially, the heterogeneous catalysts with Pd nanoparticles dispersed on various supporting materials disclosed outstanding activity[18]. The use of supports is critical for facilitating the uniform dispersion of metal catalysts with maximum utilization and preventing the metal active sites from agglomeration and loss, thus leading to further improvements in catalytic activity and stability[19,20]. In addition, the unique surface chemical and electronic properties of supports induce strong metal-support interactions, which has a great effect on improving the catalytic performance of catalysts[21,22]. Therefore, surface modification of support with selective functions is a more extensive strategy to obtain desired catalytic performance[23,24]. For instance, heteroatom (N, B, P, S) doping in the carbon can provide anchoring sites to stabilize the metal centers with uniform dispersion and introduce a strong metal-support interaction[25-29]. The introduction of N in the carbon supports has been proven active for FA dehydrogenation, in which the N atoms can anchor Pd nanoparticles on supports with good dispersion, causing an improved catalytic performance[30,31]. Moreover, the doped electronegative N atoms contribute to the surface electronic modulation of Pd nanoparticles via electron transfer, which also facilitate the efficient cleavage of C-H bonds[32,33]. Although the modification of carbon supports with the N atoms can selectively catalyze the dehydrogenation of FA, extra additives are still needed to obtain a satisfactory performance, which hinders their widespread use. In addition, amine functional groups can also be used to decorate support materials for promoting FA dehydrogenation[34-36]. It has been reported that the amine functional group has nucleophilicity and can serve as a proton scavenger to facilitate the O-H bond cleavage, thus resulting in enhanced activity in FA dehydrogenation[37,38]. Another important role of amine groups is to be used as a capping agent to protect metal nanoparticles from aggregation and growth, while it is noteworthy that more defect points will emerge as the particle size decreases, which would increase CO adsorption and cause catalyst poisoning[3]. Considering the advantages and disadvantages of the above two modifications discussed, which inspire us to combine both functionalization groups on carbon supports to construct a heterogeneous catalyst, with the synergistic promotion of Pd and nitrogen/amino groups for the FA dehydrogenation.

In this work, we propose the preparation of ultrafine Pd nanoclusters supported on nitrogen/amino co-functionalized carbon toward FA dehydrogenation. The carbon supports with abundant nitrogen-dopant atoms and amino groups enable the controllable growth of 1.42 ± 0.3 nm Pd nanoclusters with uniform dispersion. Attributing to the multiple synergies of Pd nanoclusters, nitrogen-dopant, amino groups, and

metal-support interaction, the as-prepared Pd@NH_2-NC displays excellent catalytic performance for FA dehydrogenation. Specifically, a 100 % conversion of FA into CO_2 and H_2 is completed over Pd@NH_2-NC catalyst without additive at room temperature, providing a remarkable initial turnover frequency ($TOF_{initial}$) of 4,892 h^{-1} and a low activation energy (E_a) of 28.5 kJ·mol^{-1}. These results highlight that proper multifunctional modifications of the supports have a synergistic promoting effect on catalytic reaction, providing a reference for the development of highly efficient heterogeneous catalysts.

EXPERIMENTAL

Chemicals

Sodium tetrachloropalladium (Na_2PdCl_4, 98 %), sodium borohydride ($NaBH_4$), (3-aminopropyl) triethoxysilane (APTS, 99 %), urea (AR, 99 %), and formic acid (FA, HCOOH, GR, ≥ 98 %) were purchased from Aladdin Reagents Ltd. Ethanol was purchased from FuYu Chemical Reagents. Vulcan XC-72 carbon was purchased from Cabot Carbon Ltd. All chemicals were used directly without subsequent treatment.

Preparation of nitrogen-functionalized carbon supports

Nitrogen-functionalized carbon supports (NCs) were prepared by a "soft nitriding" method according to previously reported work[39]. Typically, 1.5 g of urea was first ground into powder and mixed with 1.0 g of Vulcan XC-72 carbon in a mortar. Then, the mixed powder was placed in a crucible, then wrapped in tinfoil and heated at 150 °C for 2 h and 300 °C for another 2 h in a tube furnace. The obtained powder was repeatedly washed with water and ethanol. Finally, the as-prepared NC was dried at 60 °C overnight.

Preparation of Pd cluster supported on nitrogen/amino co-functionalized carbon (Pd@NH_2-NC)

In a typical preparation of Pd@NH_2-NC, 120 mg of NC was added to 30 mL of water under ultrasound for 1 h. Then, 0.5 mL of APTS was added to the above solution with ultrasonic treatment for 1 h and stirring for 1 h. Then, 1.0 mL of 6 mg·mL^{-1} Na_2PdCl_4 was dripped into the mixed solution. After stirring for another 2 h, 3.0 mL of $NaBH_4$ (10 mg·mL^{-1}) was introduced into the above solution, followed by stirring for 2 h. Finally, the obtained Pd@NH_2-NC was centrifuged and repeatedly washed with water, and dried at 60 °C.

The reference Pd@NH_2-C catalyst was prepared by the same process as Pd@NH_2-NC catalyst except that unfunctional carbon was used instead of NC. The reference Pd@NC catalyst was obtained with the same process as Pd@NH_2-NC catalyst but in the absence of APTS. The reference Pd@C catalyst was prepared in the same way as Pd@NH_2-NC catalyst, except for the addition of 100 mg of unfunctional carbon and in the absence of APTS.

FA dehydrogenation reaction

The reaction was carried out in a set-up as shown in Supplementary Figure 1. Typically, 160 mg of catalyst and 3.0 mL of water were mixed in the sealed round-bottom flask with ultrasonic treatment for 30 min, and then placed in a water bath at 298 K with stirring. The sealed round-bottom flask was connected to an inverted cylinder filled with water *via* a gas conduit. Then, the reaction started when 1.0 mL of FA solution (3.0 M) was injected into the round-bottom flask with a syringe. The volume of gas released was determined by the displacement of water in the cylinder over time. The displacement of water in the cylinder reached 10 mL as a unit, and the corresponding time was recorded to obtain the plots of gas volumes generated versus time. The reaction thermodynamics of FA dehydrogenation was studied by setting test temperature as 298, 303, 313, 323, and 333 K, and the kinetics of FA dehydrogenation was determined by adjusting the concentrations of Pd (5.75, 8.50, 11.25, and 14.00 mM) and the concentrations of FA (0.25, 0.50, 0.75, and 1.00 M).

For the durability tests, the equivalent of pure FA (3.0 mmol) was injected into the reaction mixture after the first dehydrogenation of FA. The resulting gas was determined by the displacement of water in the cylinder. Such a recycling process was repeated another 3 times at 298 K.

The conversion of FA (x_a) was obtained by the equation (1):

$$x_a = \frac{P_{atm}V_{gas}}{2RTn_{FA}} \quad (1)$$

Where P_{atm} is the atmospheric pressure (101325 Pa), V_{gas} refers to the volume of final released gas (CO_2 + H_2), R denotes the universal gas constant (8.3145 m^3·Pa·mol^{-1}·K^{-1}), T represents the room temperature (298 K), and n_{FA} corresponds to the mole number of FA.

The TOF values were calculated by equation (2):

$$TOF_{initial} = \frac{P_{atm}V_{gas}}{2RTn_{metal}t} \quad (2)$$

Where $TOF_{initial}$ refers to the initial turnover frequency when the conversion x_a is 20 %, n_{metal} is the total molar number of Pd in catalyst, and t represents the reaction time when x_a is 20 %. When the final reaction conversion is lower than 20 %, the $TOF_{initial}$ is based on the final conversion, which will be specified in the text.

Characterizations

Transmission electron microscopy (TEM), high-resolution transmission electron microscopy (HR-TEM), high angle annular dark field scanning transmission electron microscopy (HAADF-STEM) and energy-dispersive X-ray spectroscopy (EDS) analysis were carried out using JEOL JEM-2100 and Talos-F200X. The X-ray diffraction (XRD) patterns were acquired on a D/Max-3c (Rigaku) X-ray diffractometer by using Cu Kα radiation source (λ = 1.5406 Å). X-ray Photoelectron Spectroscopy (XPS) was carried out on a Thermo Fisher Scientific ESCALAB Xi+ spectrometer with an Al Kα radiator. Fourier infrared spectrum (FTIR) spectra were performed on Thermo Fisher Scientific Nicolet iS50 FTIR Spectrometer. The content of Pd in the catalysts was determined by a NexION 350D inductively coupled plasma atomic emission spectroscopy (ICP-MS). The Raman spectra were carried out on HR800 from HORIBA Jobin Yvon company. The contact angle measurements were performed using a DSA100 contact angle meter from KRUSS company. The composition of released gas from FA dehydrogenation was detected by a North Point NP-GC-901A gas chromatograph (GC) with a TCD and FID. A Micromeritics ASAP 2020 Plus was used to obtain nitrogen (N_2) sorption isotherms of catalysts. Raman measurements were carried out on a HR800 Raman spectrometer with a 633 nm laser excitation.

RESULTS AND DISCUSSION

The synthetic strategy of Pd nanoclusters supported on nitrogen/amino co-functionalized carbon supports is illustrated in Scheme 1. First, the NC support was prepared through a soft nitriding technique as reported[39,40]. After that, APTS was fully mixed with NC aqueous solution under ultrasonic and stirred to modify the supports with amino groups. Then, quantitative Na_2PdCl_4 aqueous solution was added to the above mixture with stirring for 2 h. After that, $NaBH_4$ solution was introduced into the above suspension and stirred for another 2 h to reduce Pd precursor. Finally, the obtained Pd@NH_2-NC was centrifuged and repeatedly washed with water. For comparison, the reference Pd@NH_2-C, Pd@NC, and Pd@C were also prepared in the same strategy.

As shown in Figure 1a, the Pd nanoclusters with ultrasmall size are uniformly dispersed on the nitrogen/amino co-functionalized carbon surface without any aggregation. The HR-TEM image shown in Figure 1b reveals a lattice spacing of 1.94 Å, corresponding to the (200) crystal face of Pd. The uniform small size (1.42 ± 0.3 nm) and good dispersion of Pd nanocluster are clearly shown in the HAADF-STEM image and particle size distributions histogram in Figure 1c and d. The TEM images of reference catalysts are also shown in Supplementary Figure 2. Obviously, Pd nanoparticles show larger size and poorer dispersion on supports for Pd@NH_2-C, Pd@NC, and Pd@C. The results indicate that the nitrogen/amino co-functionalization can provide abundant anchor sites for Pd active centers, resulting in the reduced size and uniform distribution of Pd nanoclusters on carbon supports. Furthermore, the STEM-EDS analysis in Figure 1e-h clearly demonstrates the distribution of Pd and N on carbon supports. The content of Pd in different samples is evaluated by ICP-MS, and the mass loadings of Pd in the Pd@NH_2-NC, Pd@NH_2-C, Pd@NC, and Pd@C are estimated to be 1.6 wt. %, 1.6 wt. %, 1.3 wt. %, and 2.1 wt. %, respectively. Meanwhile, the N_2 sorption isotherms of all sample show type I and type IV isotherms, suggesting that there are micropores (1.0-1.6 nm) and mesopores (larger than 4 nm) in the samples [Supplementary Figure 3]. The BET surface areas of C, Pd@C, Pd@NC, Pd@NH_2-C, Pd@NH_2-NC are measured as 238.6, 184.6, 90.4, 93.2, 78.0 $m^2 \cdot g^{-1}$, respectively.

The structural characteristics of catalysts were studied by XRD first [Figure 2a]. All catalysts reveal two broad peaks at 25° and 43° ascribed to the (002) and (101) crystal planes of amorphous carbon[41]. In addition, three clear diffraction peaks positioned at 40°, 47°, and 68° can be observed in Pd@C catalyst, which correspond to the (111), (200) and (220) planes of Pd, respectively. Notably, no significant diffraction peaks of Pd were observed for Pd@NH_2-NC, Pd@NH_2-C and Pd@NC due to the ultrasmall size of the Pd over the supports, which agrees well with the TEM characterization. Furthermore, Raman spectra display two distinct peaks at 1,338 cm^{-1} and 1,588 cm^{-1}, which are known as D and G bands, corresponding to disordered and graphitic carbon, respectively [Figure 2b]. The Pd@NH_2-NC shows a high I_D/I_G value of 1.00, which is higher than Pd@NH_2-C (0.98), Pd@NC (0.99) and Pd@C (0.91), suggesting more defects introduced by nitrogen/amino co-functionalization of carbon supports. The FT-IR spectra were performed to confirm the successful nitrogen/amino co-functionalization [Figure 2c]. As compared with Pd@C, distinguished new peaks appear at 1193 and 1721 cm^{-1} for Pd@NH_2-NC, Pd@NH_2-C, and Pd@NC, which are ascribed to the stretching of C-N and C=O groups, respectively, suggesting the successful modification of surface nitrogen[39,42]. Moreover, for the Pd@NH_2-NC and Pd@NH_2-C, the peak at 1,121 cm^{-1} originates from the asymmetric stretching of the Si-O-C bonds, and the peaks at 2,870 cm^{-1} and 2,932 cm^{-1} originate from the -CH_2- stretching from APTS, indicating the efficient graft of amino group on carbon. The photographs in Figure 2d (below) display the hydrophilicity and dispersibility of the samples in water. It is clear that Pd@NH_2-NC and Pd@NC are well dispersed in the water and remained for 60 min. In comparison, the Pd@NH_2-C and Pd@C show different degrees of sedimentation. Meanwhile, the contact angle measurements were performed to investigate the surface wettability of samples. As shown in Figure 2d

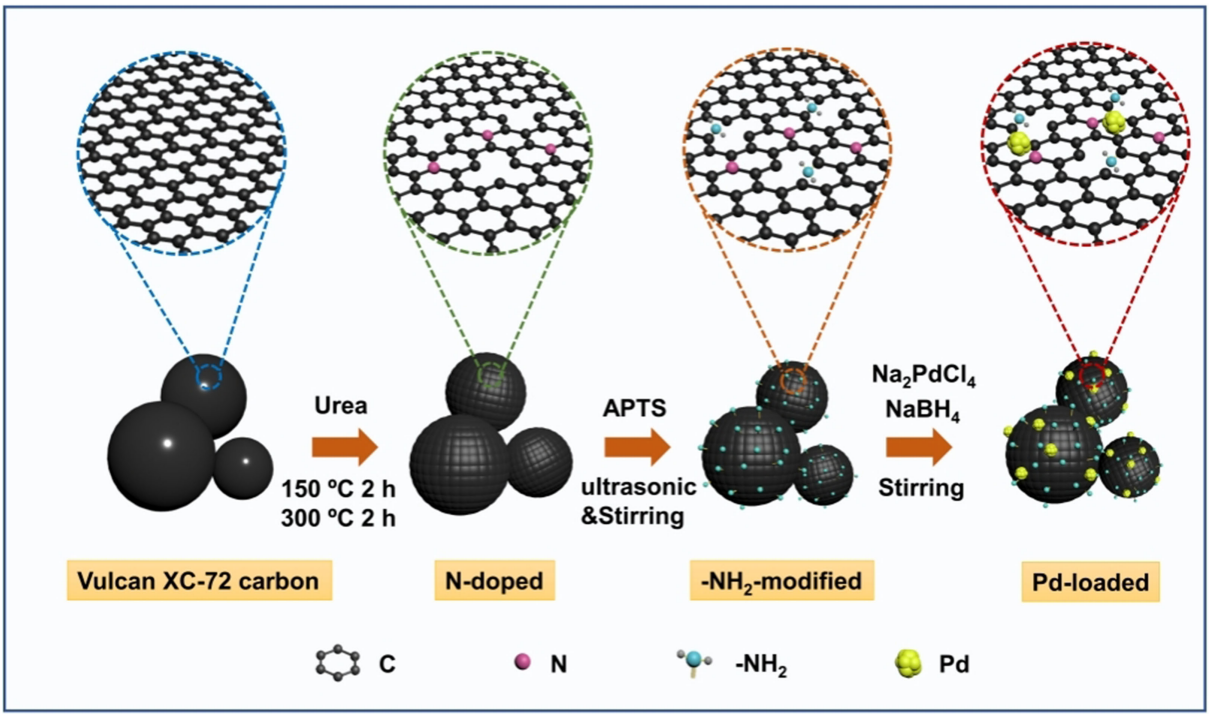

Scheme 1. A scheme illustrating the synthesis routes of Pd@NH_2-NC.

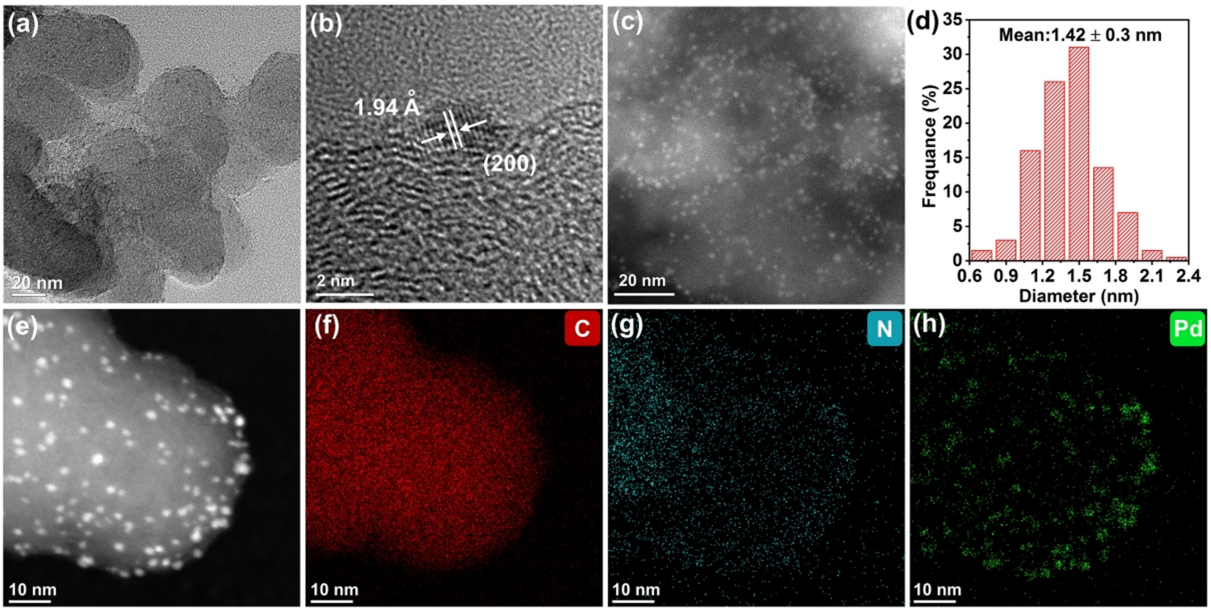

Figure 1. (a) TEM; (b) HR-TEM; (c) HAADF-STEM images; (d) particle size distributions histogram of Pd clusters; (e) HAADF-STEM image and (f-h) corresponding EDS mapping images of Pd@NH_2-NC. EDS: energy dispersive X-ray spectroscopy; HAADF-STEM: high angle annular dark field scanning transmission electron microscopy; HR-TEM: high-resolution transmission electron microscopy; TEM: Transmission electron microscopy.

(above), the Pd@C sample shows an initial water contact angle of 64.3°, and the water contact angles of Pd@NC, Pd@NH_2-C, and Pd@NH_2-NC decrease to 35.0°, 43.6°, and 36.3°, respectively. These results illustrate that the nitrogen and amino functionalization of carbon supports is efficient for enhancing the

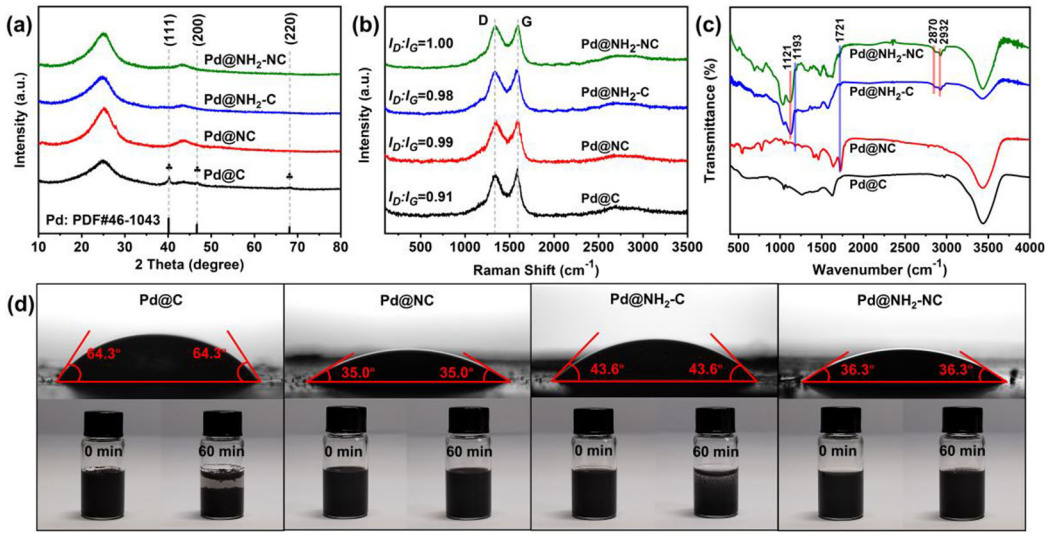

Figure 2. (a) XRD patterns; (b) Raman spectra; (c) FT-IR spectra; (d) water contact angles (above) and photographs (below) for $Pd@NH_2$-NC, $Pd@NH_2$-C, Pd@NC, and Pd@C. XRD: X-ray diffraction.

surface wettability of samples, which thus benefits the full contact between FA molecules and Pd sites and thus improves the catalytic activity.

In order to investigate the elements and corresponding chemical states, the XPS characterization of $Pd@NH_2$-NC and the reference samples was tested. The full scan spectra show that four catalysts contain C, O, and Pd, while $Pd@NH_2$-NC, $Pd@NH_2$-C, and Pd@NC also include an N element, indicating the successful nitrogen/amino functionalization of carbon supports [Figure 3a]. The nitrogen contents of $Pd@NH_2$-NC (9.2 at. %) and Pd@NC (8.1 at. %) are higher than that of $Pd@NH_2$-C (1.8 at.%), suggesting that nitrogen functionalization can greatly increase the content of nitrogen in the catalysts. The high-resolution C 1s spectra in Figure 3b display similar peaks at 284.8, 286.1, 286.6, and 288.9 eV for all samples, which are attributed to C-C, C-O, C=O, and O-C=O, respectively. For $Pd@NH_2$-NC, $Pd@NH_2$-C, and Pd@NC, a different peak at 285.6 eV corresponded to the C-N bond is observed, indicating that as-prepared samples possess the nitrogen-containing functional group[43]. From the high-resolution N 1s spectra [Figure 3c], the Pd@C displays no obvious peak, while the $Pd@NH_2$-NC, $Pd@NH_2$-C, and Pd@NC show three different nitrogen species, which are attributed to pyridinic N (at 398.8 eV), amine/amide groups (at 400.0 eV) and quaternary N (at 401.2 eV), respectively. As shown in Figure 3d, the Pd 3d spectra display a doublet and deconvolute into four peaks attributing to the Pd^0 $3d_{5/2}$, Pd^0 $3d_{3/2}$, Pd^{2+} $3d_{5/2}$ and Pd^{2+} $3d_{3/2}$, respectively. The presence of Pd^{2+} can be induced by the oxidation of the surface Pd nanoclusters in air and a large electron transfer from Pd to electronegative N/C atoms. Quantitative peak deconvolution and integration of XPS analysis show that the Pd^0 contents in $Pd@NH_2$-NC, Pd@NC, $Pd@NH_2$-C, and Pd@C are 60.02%, 10.65%, 38.83%, and 20.93%, respectively. $Pd@NH_2$-NC displays the increased Pd^0 content, suggesting the high ratio of metallic state Pd and few defects on the surface, indicating good catalytic stability[44]. In addition, the Pd^0 $3d_{5/2}$ peaks of $Pd@NH_2$-NC (336.6 eV), $Pd@NH_2$-C (336.6 eV), and Pd@NC (336.2 eV) exhibit 0.4-0.8 eV positive shift compared with Pd@C (335.8 eV), indicating the changes in the electronic structure of Pd induced by nitrogen/amino functionalization. In order to further explore the interaction between Pd and functionalized carbon support, the XPS spectra of NH_2-NC were tested and shown in Supplementary Figure 4. Relative to NH_2-NC, the binding energy of the N 1s peak in $Pd@NH_2$-NC shows a negative shift, suggesting its higher electron density after the loading of Pd nanoclusters. The shift in binding energy for N and Pd demonstrates the electron transfer from Pd to functionalized carbon

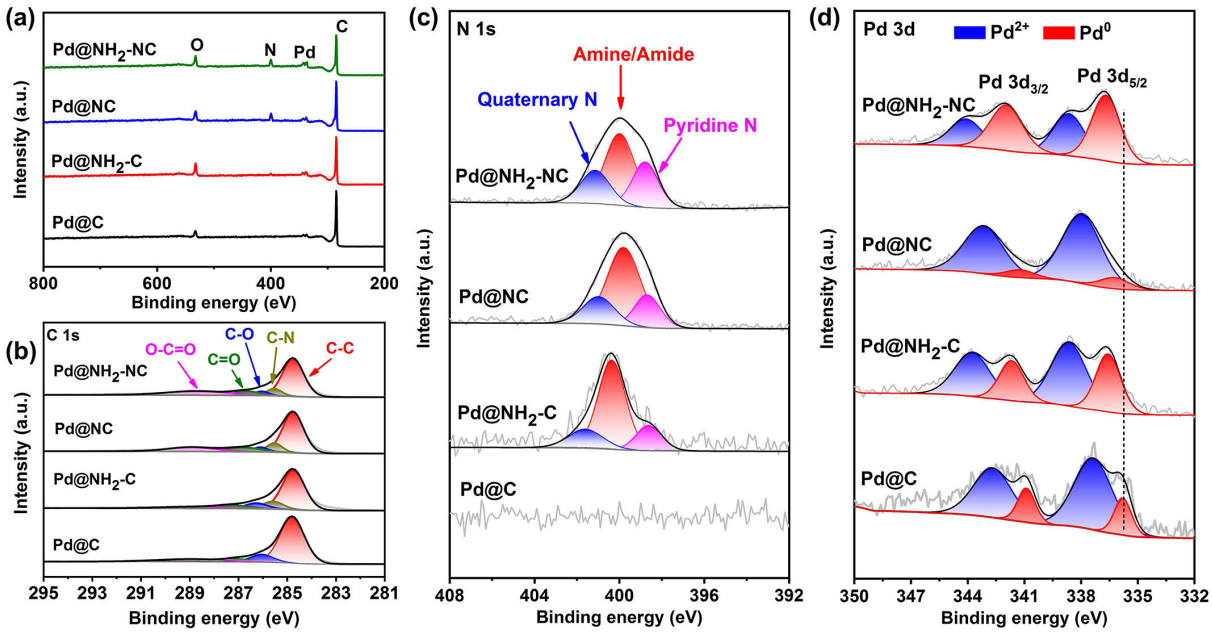

Figure 3. (a) XPS survey spectra; (b) high-resolution XPS C 1s spectra; (c) N 1s spectra; (d) Pd 3d spectra of Pd@NH_2-NC, Pd@NH_2-C, Pd@NC, and Pd@C. XPS: X-ray Photoelectron Spectroscopy.

support and proves the existence of strong metal-support interaction, which could anchor Pd nanoclusters firmly on the supports and thus improve the stability of catalysts. Meanwhile, the formed electron-deficient Pd active centers have been demonstrated to be efficient in enhancing resistance to CO poisoning and boosting the catalytic activity of FA dehydrogenation[45,46].

The catalytic performance of Pd@NH_2-NC, Pd@NH_2-C, Pd@NC, and Pd@C for dehydrogenation of FA (0.75 M, 4.0 mL) was evaluated without any additives at 298 K. Figure 4a and b show the plots of gas volumes generated versus time and corresponding $TOF_{initial}$ for above four catalysts. The Pd@NH_2-NC exhibits the best catalytic activity with 146 mL gas generated in only 2.92 min, suggesting a 100 % conversion of FA and a $TOF_{initial}$ value of 4,892 h^{-1}. In comparison, Pd@NH_2-C and Pd@NC need longer reaction times of 5.5 and 80.0 min, corresponding to the $TOF_{initial}$ values of 1,968 h^{-1} and 513 h^{-1}, respectively. In addition, Pd@C catalyst shows insufficient activity (26 h^{-1}), with 41 mL of gas released in 90 min (28 % conversion). Furthermore, the gas product released from FA dehydrogenation over Pd@NH_2-NC was detected by GC [Figure 4c]. The result displays that the generated gas consists of H_2 and CO_2, without any CO, suggesting a 100 % H_2 selectivity for FA dehydrogenation. The Raman measurements were further carried out to characterize intermediate species produced during the reaction. As shown in Supplementary Figure 5, the weak Raman peaks around 718 cm^{-1}, 1,116 cm^{-1} and 1,552 cm^{-1} could be assigned to CO_2*[47,48], while no peak of the CO* (2,035 cm^{-1}) is observed[48], which further indicate high H_2 selectivity. In addition, the dependence of the catalytic activity of the Pd@NH_2-NC catalyst on the dosage of $NaBH_4$, APTS, and urea added in the preparation process was investigated. As shown in Figure 4d-f, the Pd@NH_2-NC discloses the highest catalytic performance with the optimal dosage of $NaBH_4$ (30 mg), APTS (0.5 mL), and urea (1.5 g).

The catalytic kinetics of Pd@NH_2-NC for the dehydrogenation of FA were thoroughly investigated. Supplementary Figure 6 and Figure 5a show the time-dependent plots of the released gas and corresponding $TOF_{initial}$ under various FA concentrations. Notably, the $TOF_{initial}$ retains, with the FA concentration ranging

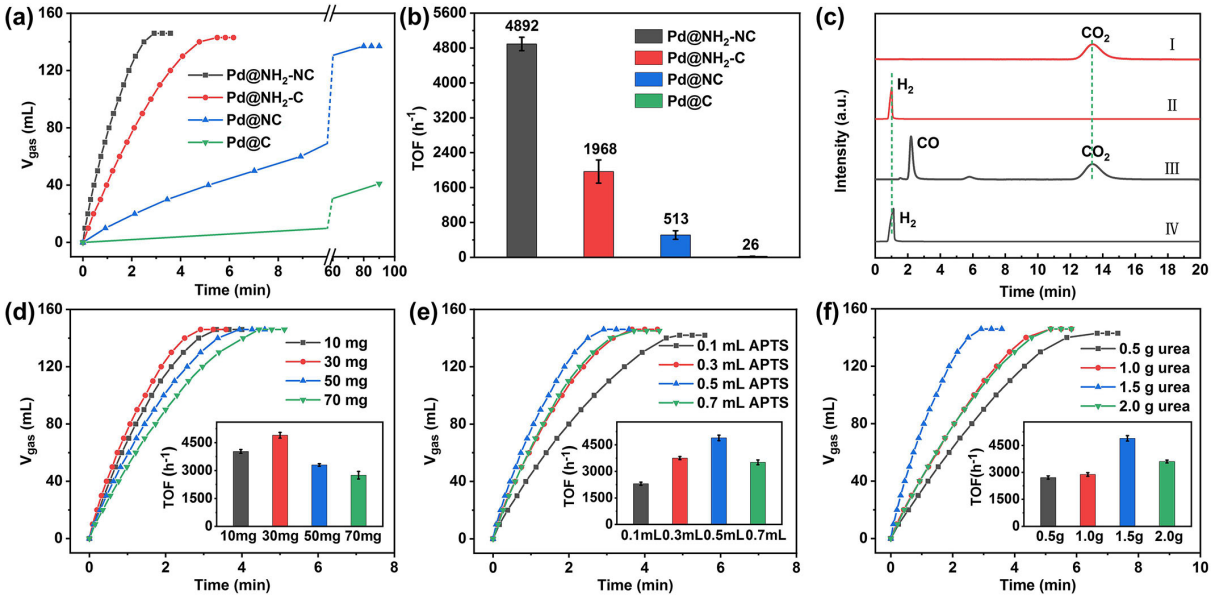

Figure 4. (a) Generated $V(H_2 + CO_2)$ versus time for the dehydrogenation of FA at 298 K and (b) corresponding TOF values over different catalysts; (c) Gas chromatography analysis results for (I, II) gas generated from FA, (III) commercial mixed standard gas containing CO and CO_2, (IV) commercial pure H_2; (d-f) Generated $V(H_2 + CO_2)$ versus time for the dehydrogenation of FA and corresponding TOF values(insets) at 298 K for Pd@NH_2-NC synthesized with (d) different amounts of $NaBH_4$, (e) different amounts of APTS, and (f) different amounts of urea. TOF: turnover frequency.

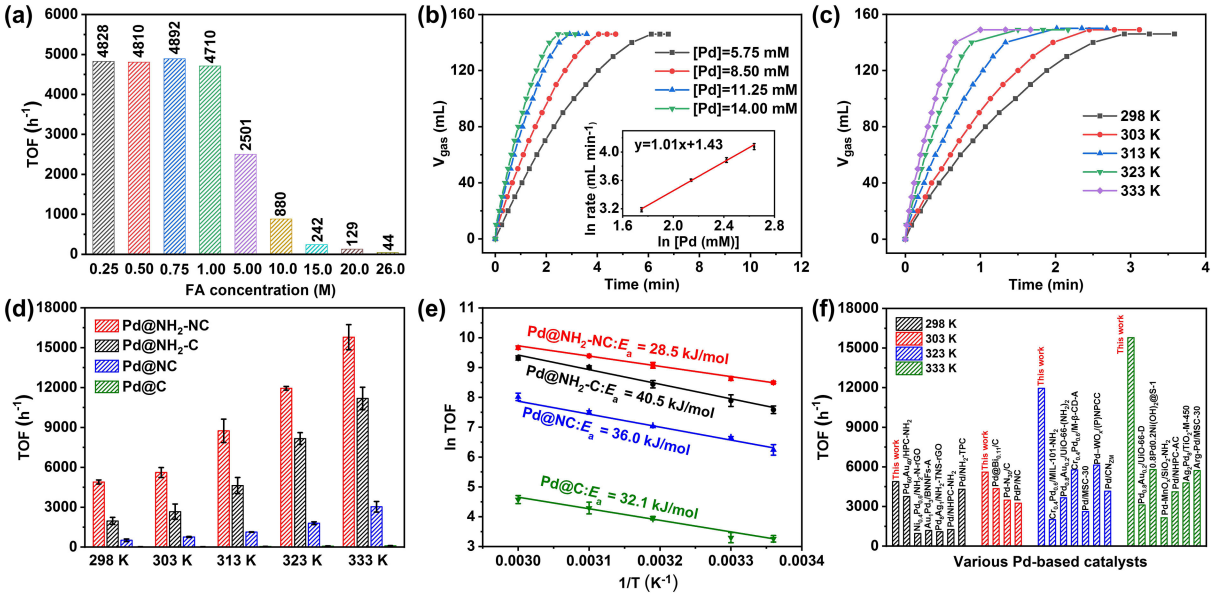

Figure 5. (a) The $TOF_{initial}$ values for the dehydrogenation of FA at 298 K over Pd@NH_2-NC with different FA concentrations (The $TOF_{initial}$ values at 20.0 M and 26.0 M were obtained when the conversion *xa* were 7.2 % and 2.7 %, respectively.); (b-c) Generated $V(H_2 + CO_2)$ versus time for the dehydrogenation of FA at 298 K over Pd@NH_2-NC with (b) different Pd concentrations (inset: the corresponding logarithmic plot of the gas generation rate versus the Pd concentration) and (c) different temperatures; (d) The TOF values of different catalysts at different temperatures and (e) corresponding Arrhenius plots (ln k versus 1/T); (f) Comparisons of catalytic activity of Pd@NH_2-NC with other reported catalysts. TOF: turnover frequency; $TOF_{initial}$: initial turnover frequency.

from 0.25 M to 1.00 M, while a sharp decrease trend of $TOF_{initial}$ is observed when the FA concentration increases from 1.00 M to 26.0 M. Meanwhile, GC results [Supplementary Figure 7] display that there is a

small amount of CO generated when the FA concentration reaches up to 15.0, 20.0, 26.0 M, suggesting that the dehydration pathways occur under the high FA concentration and thus decrease H_2 selectivity. These results indicate that the water content in the reaction system has a great influence on the catalytic performance and the H_2 selectivity, which are consistent with previous reports[49,50]. We further evaluated the dehydrogenation of FA under different amounts of catalysts [Figure 5b]. The gas production rate gradually increases when the Pd concentration increases from 5.75 to 14.00 mM. The normalized plots between In rate and In [Pd] display a slope value of 1.01, indicating that the dehydrogenation of FA over Pd@NH_2-NC catalyst is a first-order reaction in Pd concentration. The activation energy (E_a) of catalysts was also evaluated by testing the dehydrogenation of FA under elevated temperatures (298, 303, 313, 323, and 333 K). The time-dependent plots of the generated gas under different temperatures over Pd@NH_2-NC, Pd@NH_2-C, Pd@NC, and Pd@C are shown in Figure 5c and Supplementary Figure 8. The gas production rates are obviously promoted with the temperature increases. As shown in Figure 5d, the corresponding $TOF_{initial}$ values of Pd@NH_2-NC display as 4892, 5609, 8746, 11947, and 15788 h^{-1}, which are highest compared with Pd@NH_2-C, Pd@NC, and Pd@C at different temperatures. By fitting the Arrhenius plots between ln [TOF] and 1/T, the E_a value of the Pd@NH_2-NC catalyst is calculated as 28.5 kJ·mol^{-1} [Figure 5e]. In contrast, E_a values of Pd@NH_2-C, Pd@NC, and Pd@C are 40.5, 36.0, and 32.1 kJ·mol^{-1}, respectively. The lowest E_a value of Pd@NH_2-NC for FA dehydrogenation suggests the thermodynamically lowest reaction energy barrier for FA dehydrogenation. Furthermore, the $TOF_{initial}$ value of Pd@NH_2-NC is compared with other recently reported catalysts for FA dehydrogenation at 298, 323, and 333 K [Figure 5f]. Obviously, the as-prepared Pd@NH_2-NC displays higher activity than those of Pd or Pd-based alloy catalysts quoted, and details of the experimental conditions and catalytic performance of these catalysts are listed in Supplementary Table 1.

The recycling stability of the as-prepared Pd@NH_2-NC catalyst is further evaluated by re-injecting the same amount of pure FA into the previous mixture when the last reaction was completed at 298 K. As shown in Figure 6a, after five cycles, the complete dehydrogenation of FA can still be achieved with a slight decrease in gas generation rate. It only takes 10 minutes to generate 146 mL of gas in the fifth cycle, suggesting good catalytic stability of the Pd@NH_2-NC catalyst. The XRD results show a small diffraction peak at 40° for spent Pd@NH_2-NC, which indicates that the Pd nanoclusters suffer a slight aggregation with a larger particle size [Figure 6b]. Meanwhile, the TEM image of spent Pd@NH_2-NC in Figure 6c indicates that the Pd nanoclusters are still evenly distributed on the carbon surface with a slightly increased size of 1.65 ± 0.5 nm. Additionally, XPS results further show that the nitrogen content of spent Pd@NH2-NC is determined as 7.9 at. %, which is slightly lower than that of fresh Pd@NH_2-NC (9.2 at. %) [Figure 6d and Supplementary Figure 9]. There is a small amount of CO (0.23 %) for the fifth dehydrogenation of FA [Supplementary Figure 10], which may cause catalyst poisoning and lead to the reduction of circulation performance.

Based on the above studies, a possible mechanism for the dehydrogenation of FA over Pd@NH_2-NC catalyst has been proposed [Figure 7]. FA molecules are firstly absorbed on the surface of Pd@NH_2-NC, and the nitrogen/amino groups can act as proton scavengers to break the O-H bond and produce H^+, leaving $HCOO^-$ on the Pd surface[15,51]. Subsequently, the electron-deficient Pd nanoclusters induced by metal-support interaction can be active for the rupture of the C-H bond and the formation of H^-[3], followed by the release of CO_2 molecules in this process. Finally, the H^+ absorbed on amino groups combines with the H^- absorbed on Pd nanoclusters to form H_2. Therefore, the remarkable catalytic performance of Pd@NH_2-NC can be attributed to the synergistic effect of nitrogen/amino co-functionalized carbon support, Pd nanoclusters, and metal-support interaction.

CONCLUSIONS

In summary, nitrogen/amino co-functionalized carbon-supported Pd nanoclusters have been successfully

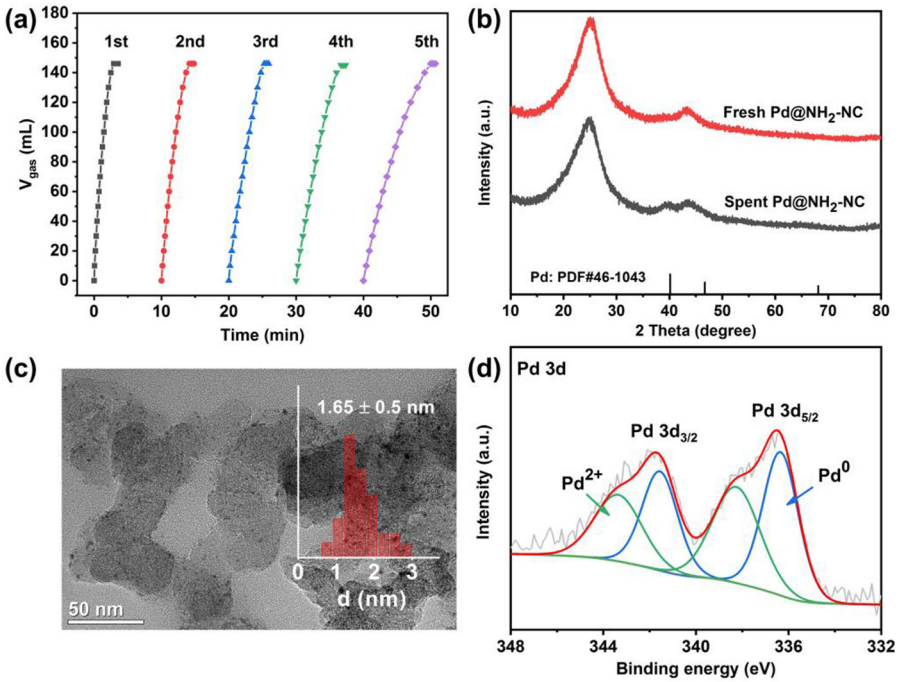

Figure 6. (a) Generated V(H_2 + CO_2) versus time for the dehydrogenation of FA over Pd@NH_2-NC from the first to fifth cycles; (b) XRD patterns of Pd@NH_2-NC before and after five cycles; (c) TEM image of Pd@NH_2-NC after five cycles (inset: Particle size distributions); (d) XPS spectrum of Pd 3d for Pd@NH_2-NC after five cycles. TEM: transmission electron microscopy; XPS: X-ray Photoelectron Spectroscopy; XRD: X-ray diffraction.

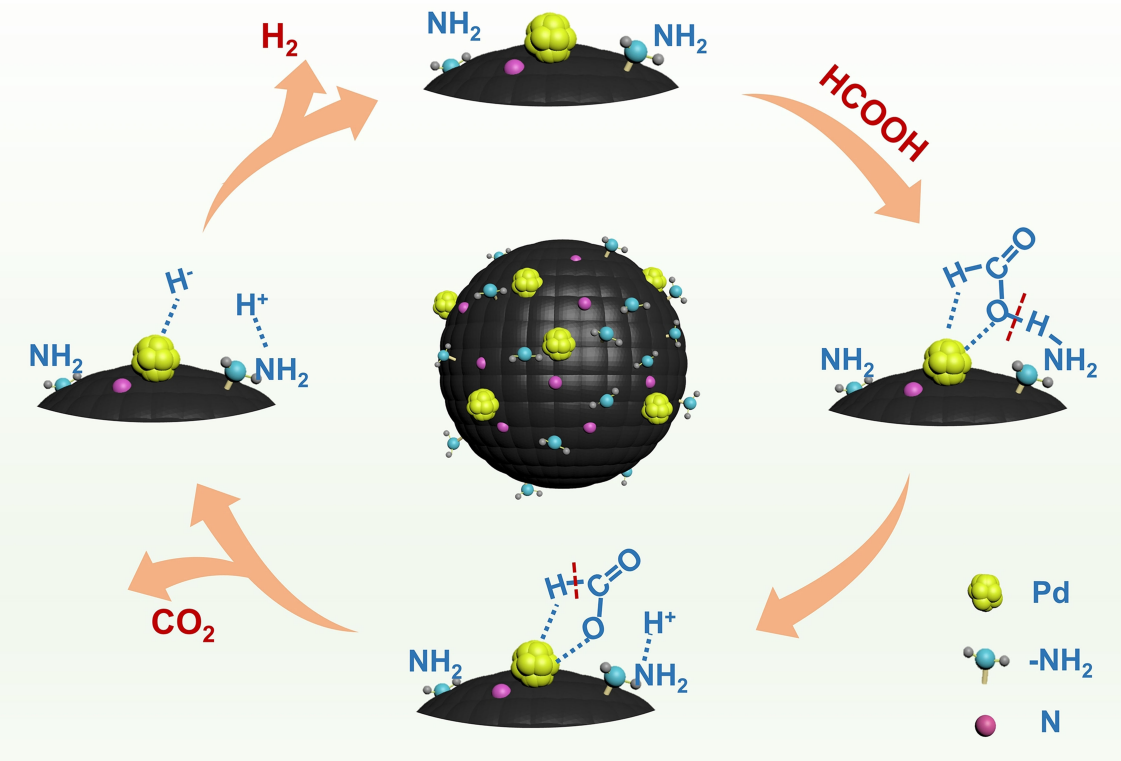

Figure 7. A possible reaction mechanism for dehydrogenation of FA over Pd@NH_2-NC. FA: formic acid.

synthesized by a simple method for efficient dehydrogenation of FA. The nitrogen/amino co-functionalization of supports endows ultrasmall Pd nanoclusters with uniform dispersion and beneficial metal-support interaction, thus enhancing catalytic reactivity. The as-prepared Pd@NH_2-NC exhibits a 100 % H_2 selectivity, with a high $TOF_{initial}$ of 4,892 h^{-1} and a low activation energy (E_a) of 28.5 kJ·mol^{-1} without additive at 298 K. In particular, $TOF_{initial}$ value of Pd@NH_2-NC reaches about 2.5 times, 9.5 times, and 188.2 times higher than that of Pd@NH_2-C, Pd@NC, and Pt/C, respectively. We expect that this work suggests a co-functionalization strategy method for the design and synthesis of carbon-supported metal catalysts with desired performance.

DECLARATIONS

Acknowledgments

We thank Mrs. Jiao Li, Yan Liang, and Jiamei Liu from the Instrument Analysis Center of Xi'an Jiaotong University for their help in obtaining TEM/ICP/XPS results.

Authors' contributions

Made substantial contributions to the conception and design of the study, performed data analysis and interpretation, and wrote original draft: Liu D, Zhou C

Conducted the investigation of the study and performed data acquisition: Wang G, Li Y

Revised the manuscript, as well as provided administrative, technical, and material support: Yang Z, Kong C, Liu B

Availability of data and materials

The detailed experimental methods and data are available from Supplementary Materials in the journal.

Financial support and sponsorship

This work was supported by the National Natural Science Foundation of China (92066207), Shccig-Qinling Program (2021JLM-27), the Innovation Capability Support Program of Shaanxi Province (2023-CX-TD-49, 2020TD-001), and Lanzhou University-Jinchuan Group Chemical Co., Ltd. Chemical Environmental Protection Industry Joint Laboratory [(20)0837].

Conflicts of interest

All authors declared that there are no conflicts of interest.

Ethical approval and consent to participate

Not applicable.

Consent for publication

Not applicable.

REFERENCES

1. Sun Q, Wang N, Xu Q, Yu J. Nanopore-supported metal nanocatalysts for efficient hydrogen generation from liquid-phase chemical hydrogen storage materials. *Adv Mater* 2020;32:e2001818. DOI PubMed
2. Mboyi CD, Poinsot D, Roger J, Fajerwerg K, Kahn ML, Hierso JC. The hydrogen-storage challenge: nanoparticles for metal-catalyzed ammonia borane dehydrogenation. *Small* 2021;17:e2102759. DOI PubMed
3. Zhong H, Iguchi M, Chatterjee M, Himeda Y, Xu Q, Kawanami H. Formic acid-based liquid organic hydrogen carrier system with heterogeneous catalysts. *Adv Sustainable Syst* 2018;2:1700161. DOI

4. Xu R, Lu W, Toan S, et al. Thermocatalytic formic acid dehydrogenation: recent advances and emerging trends. *J Mater Chem A* 2021;9:24241-60. DOI
5. Qin X, Li H, Xie S, et al. Mechanistic analysis-guided Pd-based catalysts for efficient hydrogen production from formic acid dehydrogenation. *ACS Catal* 2020;10:3921-32. DOI
6. Li X, Surkus AE, Rabeah J, et al. Cobalt single-atom catalysts with high stability for selective dehydrogenation of formic acid. *Angew Chem Int Ed Engl* 2020;59:15849-54. DOI PubMed PMC
7. Cui Y, Zhao M, Zou Y, et al. Ultrasmall AuPd nanoclusters on amine-functionalized carbon blacks as high-performance bi-functional catalysts for ethanol electrooxidation and formic acid dehydrogenation. *J Energy Chem* 2022;68:556-63. DOI
8. Wang H, Zhang B, Li X, Antonietti M, Chen J. Activating Pd nanoparticles on sol-gel prepared porous g-C_3N_4/SiO_2 *via* enlarging the Schottky barrier for efficient dehydrogenation of formic acid. *Inorg Chem Front* 2016;3:1124-9. DOI
9. Li R, Liu Z, Trinh QT, et al. Strong metal-support interaction for 2D materials: application in noble metal/TiB_2 heterointerfaces and their enhanced catalytic performance for formic acid dehydrogenation. *Adv Mater* 2021;33:e2101536. DOI PubMed
10. Zhang A, Xia J, Yao Q, Lu Z. Pd–WO_x heterostructures immobilized by MOFs-derived carbon cage for formic acid dehydrogenation. *Appl Catal B* 2022;309:121278. DOI
11. Barlocco I, Capelli S, Lu X, et al. Disclosing the role of gold on palladium-gold alloyed supported catalysts in formic acid decomposition. *ChemCatChem* 2021;13:4210-22. DOI
12. Wang Z, Liang S, Meng X, Mao S, Lian X, Wang Y. Ultrasmall PdAu alloy nanoparticles anchored on amine-functionalized hierarchically porous carbon as additive-free catalysts for highly efficient dehydrogenation of formic acid. *Appl Catal B* 2021;291:120140. DOI
13. Guo B, Li Q, Lin J, et al. Bimetallic AuPd nanoparticles loaded on amine-functionalized porous boron nitride nanofibers for catalytic dehydrogenation of formic acid. *ACS Appl Nano Mater* 2021;4:1849-57. DOI
14. Wang Z, Wang C, Mao S, Gong Y, Chen Y, Wang Y. Pd nanoparticles anchored on amino-functionalized hierarchically porous carbon for efficient dehydrogenation of formic acid under ambient conditions. *J Mater Chem A* 2019;7:25791-5. DOI
15. Shao X, Miao X, Tian F, et al. Amine-functionalized hierarchically porous carbon supported Pd nanocatalysts for highly efficient H_2 generation from formic acid with fast-diffusion channels. *J Energy Chem* 2023;76:249-58. DOI
16. Zhong S, Tsumori N, Kitta M, Xu Q. Immobilizing palladium nanoparticles on boron-oxygen-functionalized carbon nanospheres towards efficient hydrogen generation from formic acid. *Nano Res* 2019;12:2966-70. DOI
17. Deng M, Ma J, Liu Y, et al. Pd nanoparticles confined in pure Silicalite-2 zeolite with enhanced catalytic performance for the dehydrogenation of formic acid at room temperature. *Fuel* 2023;333:126466. DOI
18. Ding R, Li D, Li Y, Yu J, Jia M, Xu J. Bimetallic PdAu nanoparticles in amine-containing metal–organic framework UiO-66 for catalytic dehydrogenation of formic acid. *ACS Appl Nano Mater* 2021;4:4632-41. DOI
19. Gerber IC, Serp P. A theory/experience description of support effects in carbon-supported catalysts. *Chem Rev* 2020;120:1250-349. DOI PubMed
20. Zhang J, Ma J, Choksi TS, et al. Strong metal-support interaction boosts activity, selectivity, and stability in electrosynthesis of H_2O_2. *J Am Chem Soc* 2022;144:2255-63. DOI PubMed
21. Lin G, Ju Q, Jin Y, et al. Suppressing dissolution of Pt-based electrocatalysts through the electronic metal-support interaction. *Adv Energy Mater* 2021;11:2101050. DOI
22. Li Q, Wang X, Xie Z, et al. Polar bonds induced strong Pd-support electronic interaction drives remarkably enhanced oxygen reduction activity and stability. *Appl Catal B* 2022;305:121020. DOI
23. Dong Z, Mukhtar A, Ludwig T, et al. Efficient Pd on carbon catalyst for ammonium formate dehydrogenation: Effect of surface oxygen functional groups. *Appl Catal B* 2023;321:122015. DOI
24. Tang D, Wang T, Zhang W, Zhao Z, Zhang L, Qiao ZA. Liquid Na/K alloy interfacial synthesis of functional porous carbon at ambient temperature. *Angew Chem Int Ed Engl* 2022;61:e202203967. DOI
25. Luo Y, Chen Y, Xue Y, et al. Electronic structure regulation of iron phthalocyanine induced by anchoring on heteroatom-doping carbon sphere for efficient oxygen reduction reaction and Al-air battery. *Small* 2022;18:e2105594. DOI
26. Yang CL, Wang LN, Yin P, et al. Sulfur-anchoring synthesis of platinum intermetallic nanoparticle catalysts for fuel cells. *Science* 2021;374:459-64. DOI
27. Yu W, Huang H, Qin Y, et al. The synergistic effect of pyrrolic-N and pyridinic-N with Pt under strong metal-support interaction to achieve high-performance alkaline hydrogen evolution. *Adv Energy Mater* 2022;12:2200110. DOI
28. Yang Y, Huang H, Shen B, et al. Anchoring nanosized Pd on three-dimensional boron- and nitrogen-codoped graphene aerogels as a highly active multifunctional electrocatalyst for formic acid and methanol oxidation reactions. *Inorg Chem Front* 2020;7:700-8. DOI
29. Yuan J, Gan Y, Mou J, et al. Electrochemically induced amorphous and porous VO*x* /N-doped carbon spheres as a cathode for advanced aqueous zinc-ion batteries. *Inorg Chem Front* 2023;10:984-90. DOI
30. Wang Q, Tsumori N, Kitta M, Xu Q. Fast dehydrogenation of formic acid over palladium nanoparticles immobilized in nitrogen-doped hierarchically porous carbon. *ACS Catal* 2018;8:12041-5. DOI
31. Yu Y, Wang X, Liu C, Vladimir F, Ge J, Xing W. Surface interaction between Pd and nitrogen derived from hyperbranched polyamide towards highly effective formic acid dehydrogenation. *J Energy Chem* 2020;40:212-6. DOI
32. Bi QY, Lin JD, Liu YM, He HY, Huang FQ, Cao Y. Dehydrogenation of formic acid at room temperature: boosting palladium nanoparticle efficiency by coupling with pyridinic-nitrogen-doped carbon. *Angew Chem Int Ed Engl* 2016;55:11849-53. DOI PubMed

33. Deng M, Yang A, Ma J, et al. Enhanced catalytic performance of n-doped carbon sphere-supported pd nanoparticles by secondary nitrogen source regulation for formic acid dehydrogenation. *ACS Appl Mater Interfaces* 2022;14:18550-60. DOI
34. Ye W, Huang H, Zou W, Ge Y, Lu R, Zhang S. Controllable synthesis of supported PdAu nanoclusters and their electronic structure-dependent catalytic activity in selective dehydrogenation of formic acid. *ACS Appl Mater Interfaces* 2021;13:34258-65. DOI PubMed
35. Zhao X, Dai P, Xu D, Tao X, Liu X, Ge Q. Ultrafine PdAg alloy nanoparticles anchored on NH_2-functionalized 2D/2D TiO_2 nanosheet/rGO composite as efficient and reusable catalyst for hydrogen release from additive-free formic acid at room temperature. *J Energy Chem* 2021;59:455-64. DOI
36. Li SJ, Zhou YT, Kang X, et al. A simple and effective principle for a rational design of heterogeneous catalysts for dehydrogenation of formic acid. *Adv Mater* 2019;31:e1806781. DOI
37. Masuda S, Mori K, Futamura Y, Yamashita H. PdAg nanoparticles supported on functionalized mesoporous carbon: promotional effect of surface amine groups in reversible hydrogen delivery/storage mediated by formic acid/CO_2. *ACS Catal* 2018;8:2277-85. DOI
38. Ziaee MA, Zhong H, Cui C, Wang R. Additive-free hydrogen generation from formic acid boosted by amine-functionalized imidazolium-based ionic polymers. *ACS Sustainable Chem Eng* 2018;6:10421-8. DOI
39. Liu B, Yao H, Song W, et al. Ligand-free noble metal nanocluster catalysts on carbon supports via "soft" nitriding. *J Am Chem Soc* 2016;138:4718-21. DOI PubMed PMC
40. Lv H, Wei R, Guo X, Sun L, Liu B. Synergistic catalysis of binary RuP nanoclusters on nitrogen-functionalized hollow mesoporous carbon in hydrogen production from the hydrolysis of ammonia borane. *J Phys Chem Lett* 2021;12:696-703. DOI PubMed
41. Luo W, Zhao X, Cheng W, Zhang Y, Wang Y, Fan G. A simple and straightforward strategy for synthesis of N,P co-doped porous carbon: an efficient support for Rh nanoparticles for dehydrogenation of ammonia borane and catalytic application. *Nanoscale Adv* 2020;2:1685-93. DOI PubMed PMC
42. Yan JM, Li SJ, Yi SS, Wulan BR, Zheng WT, Jiang Q. Anchoring and upgrading ultrafine NiPd on room-temperature-synthesized bifunctional NH_2-N-rGO toward low-cost and highly efficient catalysts for selective formic acid dehydrogenation. *Adv Mater* 2018;30:e1703038. DOI PubMed
43. Li L, Li Y, Ye Y, et al. Kilogram-scale synthesis and functionalization of carbon dots for superior electrochemical potassium storage. *ACS Nano* 2021;15:6872-85. DOI
44. Duan X, Cao F, Ding R, et al. Cobalt-doping stabilized active and durable sub-2 nm Pt nanoclusters for low-Pt-loading PEMFC cathode. *Adv Energy Mater* 2022;12:2103144. DOI
45. Ye W, Pei W, Zhou S, et al. Controlling the synthesis of uniform electron-deficient Pd clusters for superior hydrogen production from formic acid. *J Mater Chem A* 2019;7:10363-71. DOI
46. Chang J, Wang G, Chang X, et al. Interface synergism and engineering of Pd/Co@N-C for direct ethanol fuel cells. *Nat Commun* 2023;14:1346. DOI PubMed PMC
47. Zhao Y, Zhang X, Bodappa N, et al. Elucidating electrochemical CO_2 reduction reaction processes on Cu(*hkl*) single-crystal surfaces by *in situ* Raman spectroscopy. *Energy Environ Sci* 2022;15:3968-77. DOI
48. Shan W, Liu R, Zhao H, et al. *In Situ* surface-enhanced raman spectroscopic evidence on the origin of selectivity in CO_2 electrocatalytic reduction. *ACS Nano* 2020;14:11363-72. DOI PubMed
49. Yu Z, Yang Y, Yang S, et al. Selective dehydrogenation of aqueous formic acid over multifunctional γ-Mo_2N catalysts at a temperature lower than 100 ℃. *Appl Catal B* 2022;313:121445. DOI
50. Zhu H, Wong RJ, Du X, et al. Synergistic effect of PtNi alloy loading on TiB_2 to construct SMSI catalysing formic acid dehydrogenation. *Sustain Energy Fuels* 2022;6:5531-8. DOI
51. Li Z, Yang X, Tsumori N, et al. Tandem nitrogen functionalization of porous carbon: toward immobilizing highly active palladium nanoclusters for dehydrogenation of formic acid. *ACS Catal* 2017;7:2720-4. DOI